Bingham Characteristics of Polymer-Based Electrorheological Fluids with Different Electrode Gaps and Materials

S. B. Choi,[1] Y. M. Han,[1] J. W. Sohn,[1] H. J. Choi[2]

[1]*Smart Structures and Systems Laboratory, Department of Mechanical Engineering, Inha University, Incheon 402-751, Korea*
[2]*Department of Polymer Science and Engineering, Inha University, Incheon 402-751, Korea*

Received 1 September 2008; accepted 27 June 2009
DOI 10.1002/app.31036
Published online 12 August 2009 in Wiley InterScience (www.interscience.wiley.com).

ABSTRACT: This article presents experimental results on the influence of the electrode gap and electrode material on the Bingham characteristics of polymer-based electrorheological (ER) fluids. An experimental apparatus adaptable to various types of electrodes was established for this investigation. Three different electrode gaps and three different electrode materials were tested. For ER fluids, a water-based Arabic gum ER fluid and a dry-based polyurethane ER fluid were tested. The field-dependent yield stresses and current densities were demonstrated under various operating temperatures. In addition, time responses of the ER fluids were experimentally investigated for on–off states of an input electric field and at different operating temperatures. © 2009 Wiley Periodicals, Inc. J Appl Polym Sci 114: 3636–3644, 2009

Key words: polysaccharides; rheology; viscoelastic properties

INTRODUCTION

Electrorheological (ER) fluids belong to a class of colloidal suspensions that exhibit reversible changes in their rheological behavior when subjected to external electric fields.[1,2] Since Winslow[3] reported on ER fluids, many researchers have actively studied the materials, mechanisms, and applications of ER fluids. One of the salient properties of ER fluids is that they have a very fast response to electric fields, hence providing wide control bandwidth in addition to enhanced structural and rheological properties such as yield stress, shear viscosity, and dynamic modulus.[4,5] This inherent feature has triggered tremendous research activity in the development of various engineering applications, including torque transducers, dampers, actuators, and other control systems. In general, the working behavior of actuators based on ER fluids is classified into three different working modes: shear, flow, and squeeze.[6] In the shear mode, one of the two electrodes, whose gap is filled with ER fluids, is free to translate or rotate against the other. Application devices operated under the shear mode include clutches and brakes.[7,8] In the flow mode, ER fluids flow between two fixed electrodes. Pressure drops can be controlled by an electric field in this mode, and thus vibration dampers can be realized.[9,10] Unlike in the former two modes, the electrode gap in the squeeze mode is varied, and the ER fluid is squeezed by a normal force. This mode is very effective for suppressing the vibrations featured by high frequencies and low amplitudes.[11–13]

The successful development of ER fluid technology essentially requires three principal ingredients: an advanced ER fluid, a reliable mechanism, and an efficacious control algorithm. An advanced ER fluid features high field-dependent yield stress and low viscosity in the absence of an electric field. Numerous works have contributed to the development of advanced ER fluids, including both wet-based and dry-based suspensions.[14–16] In wet-based systems featuring hydrophilic particles such as starch, silica particles, and cellulose,[17] the particle chain structure develops by either the polarization of the water or the migration of ions in the absorbed water. Several disadvantages of this system, such as water evaporation, corrosion, and a limited range of operating temperatures, have been noted. Concurrently, various promising materials for ER fluids, including zeolite,[18] carbonaceous particles,[19] starch phosphate,[20] and semiconducting polymers such as sulfonated poly (styrene-*co*-divinylbenzene),[21] camphorsulfonic acid/polyaniline,[22] polyaniline and copolyaniline, and polymer–clay nanocomposites,[23–28] have been widely adopted as materials for dry-based, nearly anhydrous

Correspondence to: H. J. Choi (hjchoi@inha.ac.kr).
Contract grant sponsor: Korea Science and Engineering Foundation; contract grant number: R17-2007-028-01000-0.

ER fluids. In addition to the effort to improve the field-dependent yield stress, research on the temperature sensitivity and durability of ER fluids has been undertaken to provide practical flavor.[29,30]

An efficacious control algorithm features control accuracy and control robustness for an ER system subjected to parameter uncertainties and external disturbances. To achieve this objective, various control strategies have been developed and implemented.[8,31,32] The reliability of the mechanism is directly influenced by the choice of the electrode materials as well as the design configuration. The two most important design parameters for ER devices or mechanism development are the electrode material and electrode gap. These parameters significantly affect the yield stress, power consumption, and mechanism reliability. Thus far, there have been no reports on the influence of different electrode materials and electrode gaps on the Bingham properties of ER fluids.

Consequently, the main contribution of this work is to experimentally show the field-dependent Bingham and response characteristics of ER fluids with respect to different electrode gaps and materials. To achieve this goal, an experimental apparatus adaptable to the various gaps and materials was designed and manufactured. The field-dependent yield stresses, current densities, and response times were measured and compared among different electrode gaps (0.75, 1.00, and 1.25 mm), electrode materials (stainless steel, carbon steel, and brass), and ER fluids under operating temperatures of 25, 70, and 100°C.

EXPERIMENTAL

Materials

Two kinds of ER fluids were chosen for the comparison of Bingham response characteristics. One was a water-based ER fluid (ERF-1) made from Arabic gum and transformer oil as the particles and base liquid, respectively. The size of the particles ranged from 10 to 60 μm, and the dynamic viscosity of the oil was 10 cS. The weight ratio of the particles to the ER fluid was 30%.[33] The Arabic gum particles were milled in a grinder to produce particle sizes of less than 60 μm and dried in a thermohygrostat chamber for 1 day before mixing. On the other hand, a dry-based polyurethane ER fluid (ERF-2) was purchased from Bayer (Germany); polyurethane-based ionic conductor particles were used as the dispersed phase of the ER fluid. It was reported that polymers based on functional polyethers as well as aliphatic polyesters and polycarbonate were crosslinked with isocyanates to form polyurethane elastomers with the dimensional stability required for the dispersed phase of an ER fluid in silicone oil.[34]

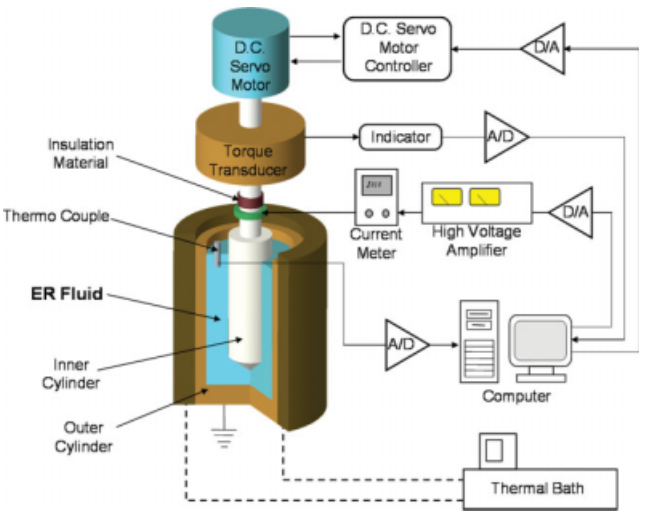

Figure 1 Schematic diagram of the experimental apparatus (D/A = digital to analog). [Color figure can be viewed in the online issue, which is available at www.interscience.wiley.com.]

Apparatus

As for the apparatus, Figure 1 shows a rotational shear-mode-type electroviscometer designed and manufactured to measure the yield stress, current density, and response time with respect to the input electric field. Each electrode is composed of inner and outer cylinders connected to a power source and an electric ground, respectively. The inner cylinder rotates by means of a controlled direct-current (dc) servomotor to get shear rates of up to 2000 s^{-1}, whereas the outer cylinder is fixed. The torque is measured by a strain-gauge-type torque transducer directly connected to the dc servomotor and converted to the corresponding shear stress. The analog-to-digital (A/D) converter has a 12-bit resolution. The operating program is written in the C++ language and is executed with a sampling time of 1200 Hz. Therefore, the fast response time of the ER fluid, which is hard to measure with a commercial viscometer, can be measured with the testing device manufactured in this work. The high-voltage amplifier has a dynamic bandwidth above 1500 Hz.

The schematic configuration of the cylindrical electrode is given in Figure 2. In the steady rotational mode, the inner cylinder rotates at a controllable constant speed. The torque on the stationary outer cylinder and the rotational velocity of the inner cylinder are measured for the determination of the shear stress and shear rate. Once the torque (T) is measured, it is simple to describe the fluid shear stress ($\tau_{r\theta}$) at any point with the radius (r) between the two cylinders:

$$\tau_{r\theta} = \frac{T}{2\pi r^2 L C_L} \quad (1)$$

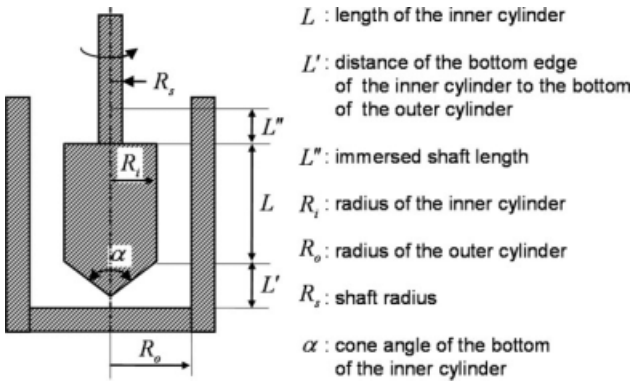

Figure 2 Schematic configuration of the electrode.

where C_L is the resistance coefficient of surface correction, which is normally determined in an empirical manner. In this work, this value was determined to be 1.1 by a comparison of the relationship between the shear stress and torque of the proposed device with that of a commercial device (VT1000, Physica, Stuttgart, Germany). The length of the inner cylinder (L) takes into account the so-called end effects.[35] For non-Newtonian fluids, when the inner cylinder rotates with ω (frequency) around the stationary outer cylinder, the fluid velocity and shear rate profiles are obtained from the momentum equation as follows.

$$v_\theta(r) = \frac{R_i\omega}{1-(R_i/R_o)^{2/n}}\left[\frac{r}{R_i} - \left(\frac{r}{R_i}\right)^{1-2/n}\right] \quad (2)$$

$$\dot{\gamma}_{r\theta}(r) = r\frac{\partial}{\partial r}\left(\frac{v_\theta}{r}\right) = \omega\left(\frac{2}{n}\right)\frac{1}{\delta^{2/n}-1}\left(\frac{R_o}{r}\right)^{2/n} \quad (3)$$

where $\dot{\gamma}_{r\theta}(r)$ is shear rate, $v(r)$ is fluid velocity, δ is the bob radius ratio ($\delta = R_o/R_i$), R_o is the radius of the outer cylinder, and R_i is the radius of the inner cylinder. Exponent n is the flow behavior index.

For any fluid, including non-Newtonian fluids, there is a radius at which the shear rate is virtually independent of the fluid type for the given value of ω. This radius is a function of geometry only. It is called the representative radius (R_R) and is determined with eq. (1) as the location corresponding to the so-called representative shear stress (τ_R), which is the average of the stresses at the inner and outer cylinders [$\tau_R = (\tau_i + \tau_o)/2$]. The radius is given by

$$R_R = R_i\sqrt{\frac{2\delta^2}{1+\delta^2}} = R_o\sqrt{\frac{2}{1+\delta^2}} \quad (4)$$

Because τ_R and the shear rate at R_R ($\dot{\gamma}_R$) are virtually independent of the fluid type, τ_R and $\dot{\gamma}_R$ are calculated for a Newtonian fluid ($n = 1$) at $r = R_R$ from eqs. (1), (3), and (4):

$$\dot{\gamma}_R = \frac{\delta^2+1}{\delta^2-1}\frac{2\pi\cdot N}{60} = I_{sr}\frac{2\pi\cdot N}{60} \quad (5)$$

$$\tau_R = \frac{\delta^2+1}{2\delta^2}\frac{T}{2\pi R_i^2 L C_L} = I_{ss}\frac{T}{2\pi R_i^2 L C_L} \quad (6)$$

where N is the number of revolutions and I_{ss} and I_{sr} are the influence coefficients of δ on the shear stress and shear rate, respectively.

The accuracy of the representative parameters depends on the geometry of the cylinders (δ) and on n. According to German standards,[28] $\delta = R_o/R_i$ should be equal to or less than 1.1. The maximum error between $\dot{\gamma}_R$ and $\dot{\gamma}_{r\theta}$ is less than 0.2% for a wide range of fluid types ($0.35 < n < 3.5$).

The manufactured electroviscometer is adaptable to different gaps and materials. To validate the reliability of the manufactured electroviscometer, the yield stress of a specific ER fluid was obtained with respect to electric field intensities and then compared with results obtained from a commercial rheometer (VT1000, Physica). Figure 3 shows the measured torque, from which the yield stress could be calculated. As shown in the figure, the applied electric field increased in a stepwise manner, and each step was maintained for 1 s to satisfy steady-state conditions. In the mean time, the shear rate was fixed at a certain value.

Figure 4 presents the shear stress calculated from the measured torque. This shear stress was used to obtain a linear regression. The dynamic yield stress of an ER fluid obtained from the intercept at zero shear rates is nearly independent of the shear rate. These properties, of course, depend on the type of ER fluid, operating temperature, and so forth. In Figure 5, experimental results of the yield stress measured by the proposed viscometer and a commercial viscometer are compared. The difference in the yield stresses is within the boundary of error and hence is acceptable. From these results, it can be guaranteed

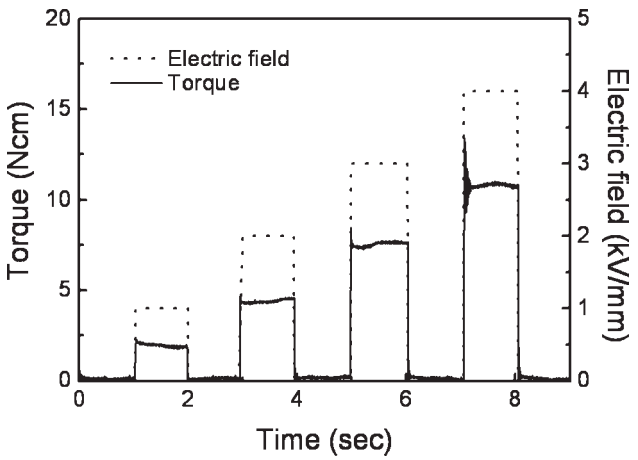

Figure 3 Field-dependent torque of an ER fluid.

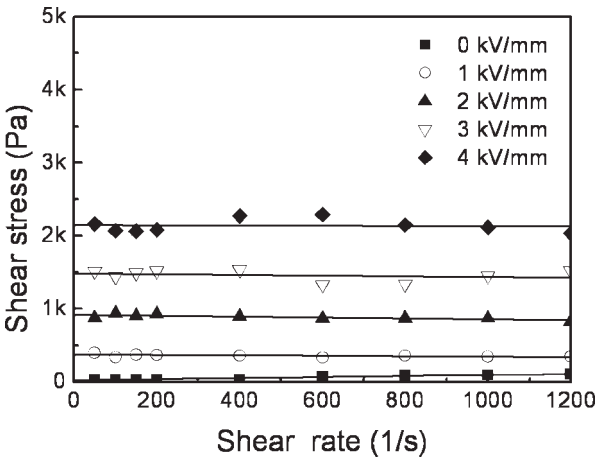

Figure 4 Shear stress of an ER fluid.

that the manufactured electroviscometer provides highly reliable Bingham properties.

In addition, information on the current density (J) is very important to determine the power consumption characteristics (voltage and current limit) of the high-voltage amplifier, which normally has an amplification factor of 1000. J of an ER fluid is known to have the following relation with respect to the electric field (E):

$$J = aE^b \tag{7}$$

where the values of a and b can be experimentally determined under various conditions.

RESULTS AND DISCUSSION

An ER fluid undergoes reversible changes in its rheological properties when it is subjected to an electric field. The most significant change is associated with the yield stress of the suspension particles, which are aligned in chains by the imposition of the electric field on the fluid domain. An ER fluid, in general, is modeled as a Bingham fluid, the constitutive equation of which is expressed as follows[4,36]:

$$\tau = \eta\dot{\gamma} + \tau_y(E) \tag{8}$$

where τ is the shear stress; $\dot{\gamma}$ is the shear rate; η is the viscosity of the ER fluid; and $\tau_y(E)$ is the yield stress of the ER fluid, which is a function of electric field E. The yield stress of an ER fluid means the shear stress of the moment at which the ER fluid starts flowing. However, it is hard to accurately measure the yield stress of an ER fluid. Therefore, the intercept value by means of the interpolation of the shear stress is often adopted as a dynamic yield stress. In general, the dynamic yield stress has been treated as $\tau_y(E)$ of the ER fluid, which exponentially increases with respect to the electric field.[5] Therefore, eq. (8) can be represented by

$$\tau = \eta\dot{\gamma} + \alpha E^\beta \tag{9}$$

where coefficient α and exponent β are experimentally determined intrinsic values of an ER fluid affected by the particle size, particle shape, particle concentration, carrier liquid, water content, temperature, and so on.

In this work, the influence of the electrode gap and electrode material on the Bingham characteristics of ER fluids was experimentally evaluated with the manufactured electroviscometer. Figure 6 shows the manufactured inner and outer electrodes used in the test. In this work, nine different electrode sets were manufactured with three different electrode gaps (0.75, 1.00, and 1.25 mm) and three different electrode materials (stainless steel, carbon steel, and brass). For each electrode set, the inner diameter of the outer cylinder and the length of the inner cylinder were 28 and 40 mm, respectively.

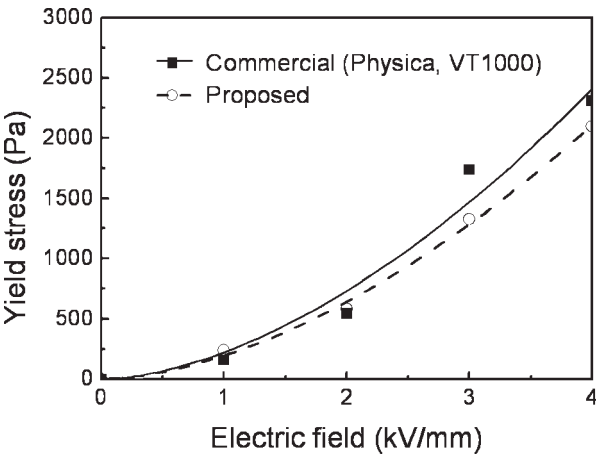

Figure 5 Comparison of the yield shear stress with two different electroviscometers.

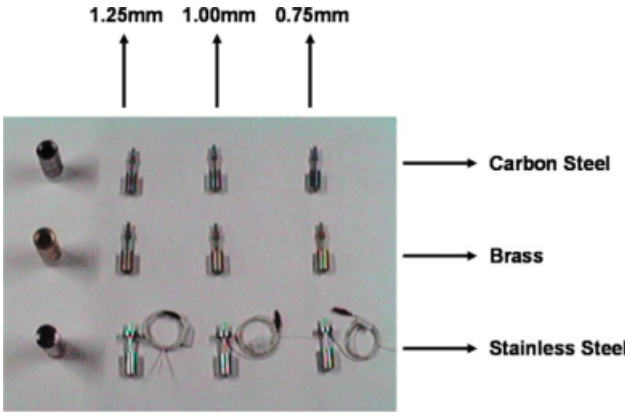

Figure 6 Manufactured cylindrical electrodes. [Color figure can be viewed in the online issue, which is available at www.interscience.wiley.com.]

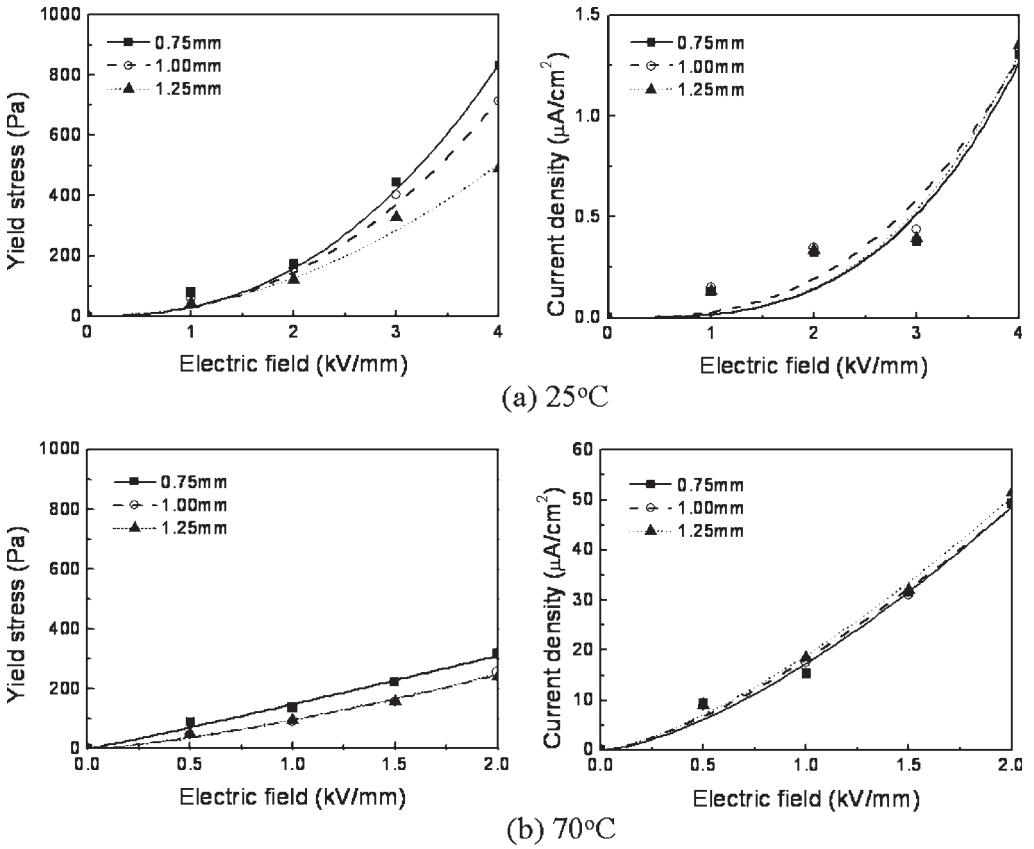

Figure 7 Bingham characteristics of ERF-1 with different gaps.

Before the experimental investigation of the Bingham characteristics, the variation of the shear stress and shear rate with respect to the electrode gap was evaluated with the following radius ratios:

$$\begin{aligned}\delta_{0.75} &= \frac{14}{13.25} = 1.056604 \\ \delta_{1.00} &= \frac{14}{13.00} = 1.076923 \\ \delta_{1.25} &= \frac{14}{12.75} = 1.098039\end{aligned} \tag{10}$$

Substituting these ratios into eq. (6), we can obtain the relationship between the torque and shear stress as follows:

$$\begin{aligned}\tau_{0.75} &= I_{ss,0.75}\frac{T}{2\pi LR_i^2C_L} = 0.9478635\frac{T}{2\pi LR_i^2C_L} \\ &= 0.0000195T \ (R_i = 13.25) \\ \tau_{1.00} &= I_{ss,1.00}\frac{T}{2\pi LR_i^2C_L} = 0.9311224\frac{T}{2\pi LR_i^2C_L} \\ &= 0.0000199T \ (R_i = 13.00) \\ \tau_{1.25} &= I_{ss,1.25}\frac{T}{2\pi LR_i^2C_L} = 0.9147003\frac{T}{2\pi LR_i^2C_L} \\ &= 0.0000204T \ (R_i = 12.75)\end{aligned} \tag{11}$$

Furthermore, the shear rate can be expressed by the substitution of eq. (10) into eq. (5) as follows:

$$\begin{aligned}\dot{\gamma}_{0.75} &= I_{sr,0.75}\frac{2\pi\cdot N}{60} = 18.1804281\frac{2\pi\cdot N}{60} = 1.9038500N \\ \dot{\gamma}_{1.00} &= I_{sr,1.00}\frac{2\pi\cdot N}{60} = 13.5185185\frac{2\pi\cdot N}{60} = 1.4156559N \\ \dot{\gamma}_{1.25} &= I_{sr,1.25}\frac{2\pi\cdot N}{60} = 10.7233645\frac{2\pi\cdot N}{60} = 1.1229481N\end{aligned} \tag{12}$$

Consequently, the shear stresses show almost the same values with respect to the electrode gaps in cases in which the measured torques are equal. However, the revolution speed of the motor should be increased as the electrode gap increases to maintain an equal shear rate.

To explicitly observe the influence of the electrode gap, the variations of the field-dependent yield stress and current density were evaluated for three different electrode gaps: 0.75, 1.00, and 1.25 mm. The experimental results for the Bingham properties with ERF-1 are presented in Figure 7. According to the results with an operating temperature of 25°C, as shown in Figure 7(a), the yield stress at 4 kV/mm increased from 429 Pa at the electrode gap of 1.25 mm up to 714 Pa at 1.00 mm and 830 Pa at

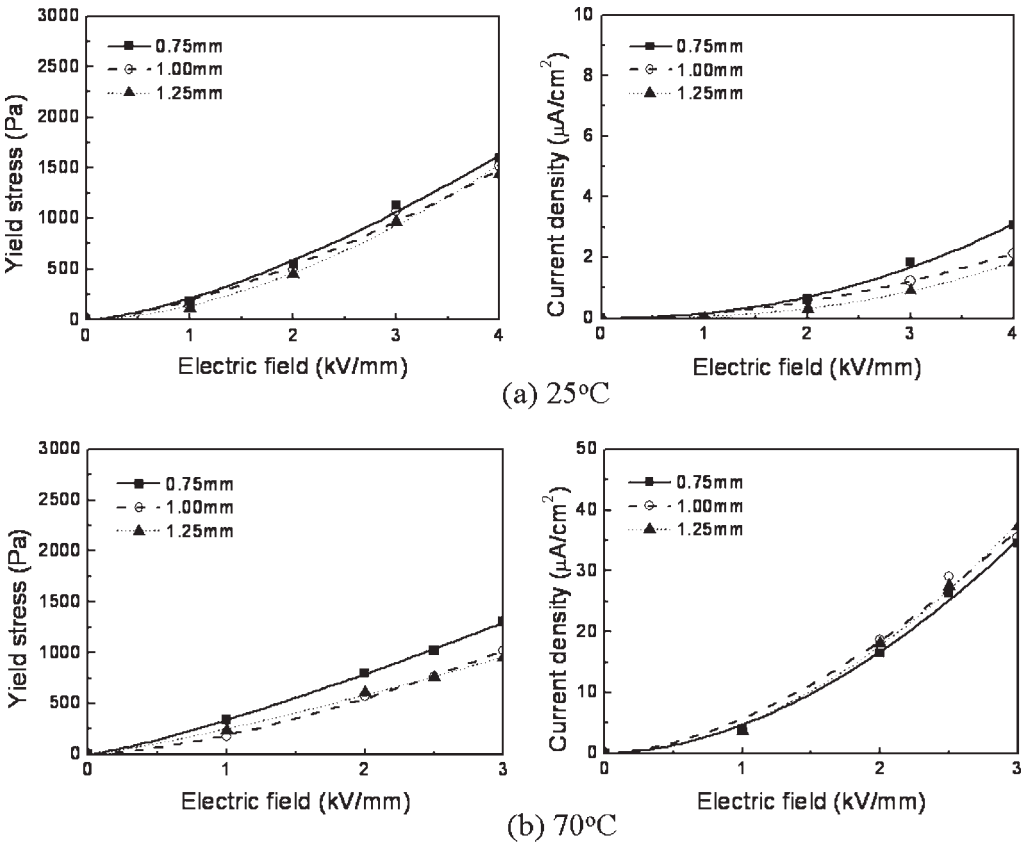

Figure 8 Bingham characteristics of ERF-2 with different gaps.

0.75 mm. In the mean time, the current densities of the three different electrode gaps were quite similar. Therefore, it can be inferred that the smaller electrode gap is more efficient than the large one because higher yield stress can be obtained with the same power consumption with the smaller electrode gap. Figure 7(b) shows experimental results at 70°C. The yield stress was higher than at 25°C. However, the maximum yield stress was low because the electric field was restricted by 2 kV/mm. This was because the increased current density caused power consumption to exceed the limit of the power amplifier (voltage range = 10 kV, current range = 10 mA).

Figure 8 shows experimental results with ERF-2, which is a dry-based ER fluid. As was the case for ERF-1, the maximum yield stress of ERF-2 was obtained from the smallest electrode gap of 0.75 mm at both 25 and 70°C. However, the yield stress at 25°C was not much affected by the variation of the electrode gap, whereas the current density was increased a little by a reduction of the gap. Furthermore, the maximum yield stress at 70°C was almost the same as that at 25°C even though the current density increased by 10 times. Thus, it can be seen that the ratio of the efficiency of the yield stress to power consumption was reduced with an increase in the temperature. Consequently, the yield stresses of ERF-1 and ERF-2 increased as the electrode gap decreased. However, the yield stresses of ERF-1 and ERF-2 were maintained as the operating temperature increased, but the maximum yield stress decreased because of limitations of the electric field caused by the high current density. In addition, the applied electric fields were subjected to high current densities at a high operating temperature, regardless of electrode gaps.

The influence of the electrode materials on the Bingham characteristics was evaluated for three different materials: stainless steel, carbon steel, and brass. The experimental results with ERF-1 are presented in Figure 9. The maximum yield stress was produced by the stainless steel electrode at 25°C because the electric fields for the carbon steel and brass electrodes were limited by 3.5 kV/mm on account of the high current density. As the operating temperature increased from 25 to 70°C, the maximum yield stress of the stainless steel electrode decreased from 714.1 Pa at 4 kV/mm to 250 Pa at 2 kV/mm, whereas the maximum yield stresses of the carbon steel and brass electrodes were not much changed, even though their electric fields were reduced to 2.5 and 3 kV/mm, respectively. This was mainly caused by the fact that the current density of the stainless steel electrode was highly subject to the operating temperature, as shown in the results.

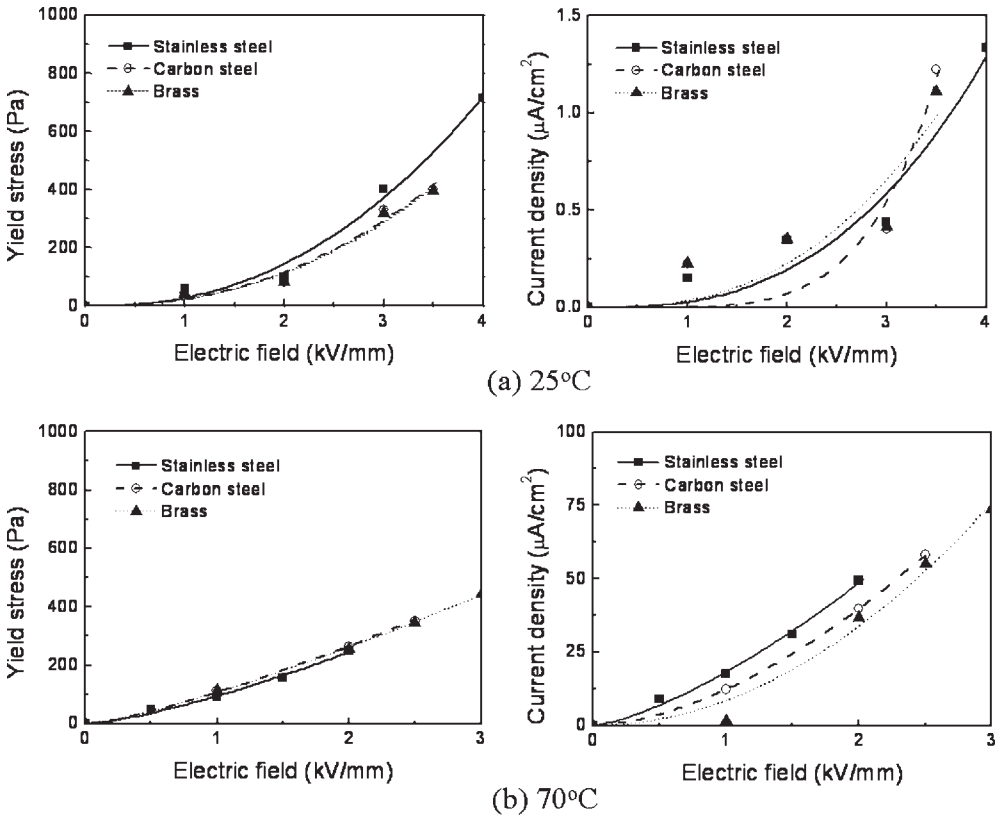

Figure 9 Bingham characteristics of ERF-1 with different electrode materials.

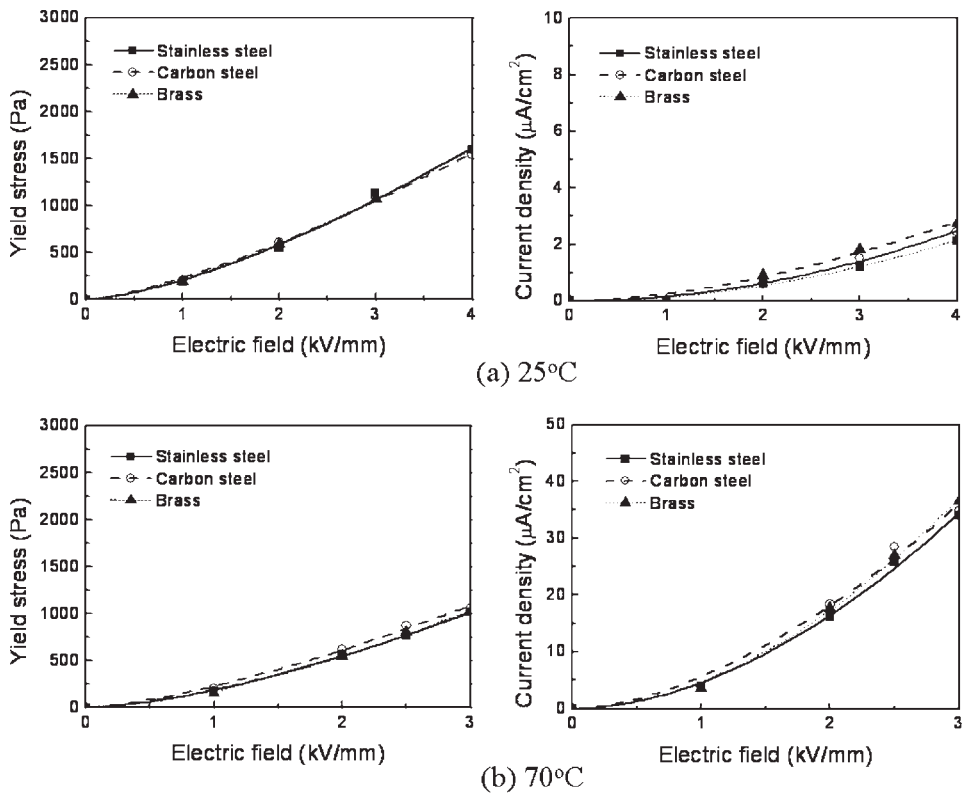

Figure 10 Bingham characteristics of ERF-2 with different electrode materials.

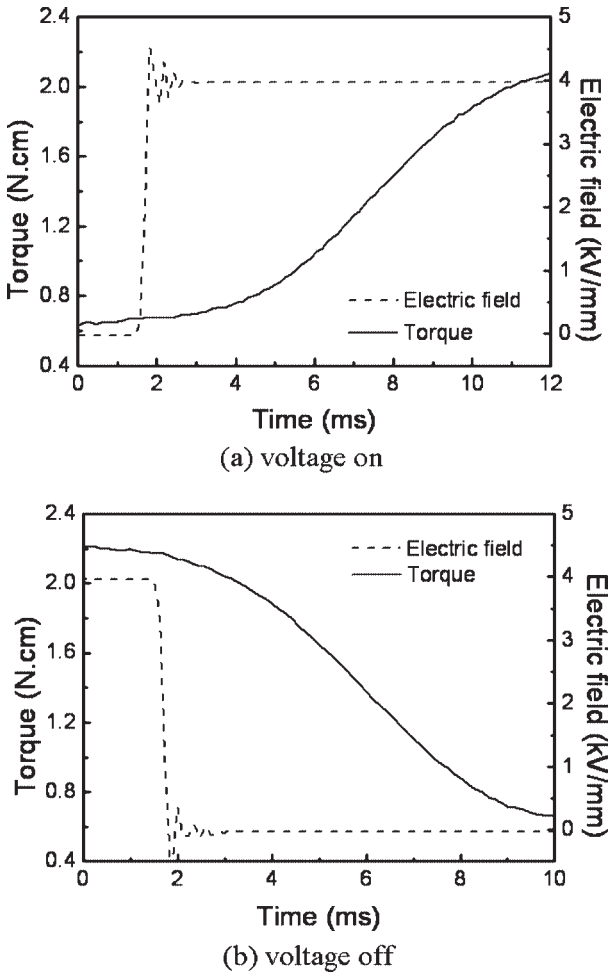

Figure 11 Response time of ERF-1 (25°C).

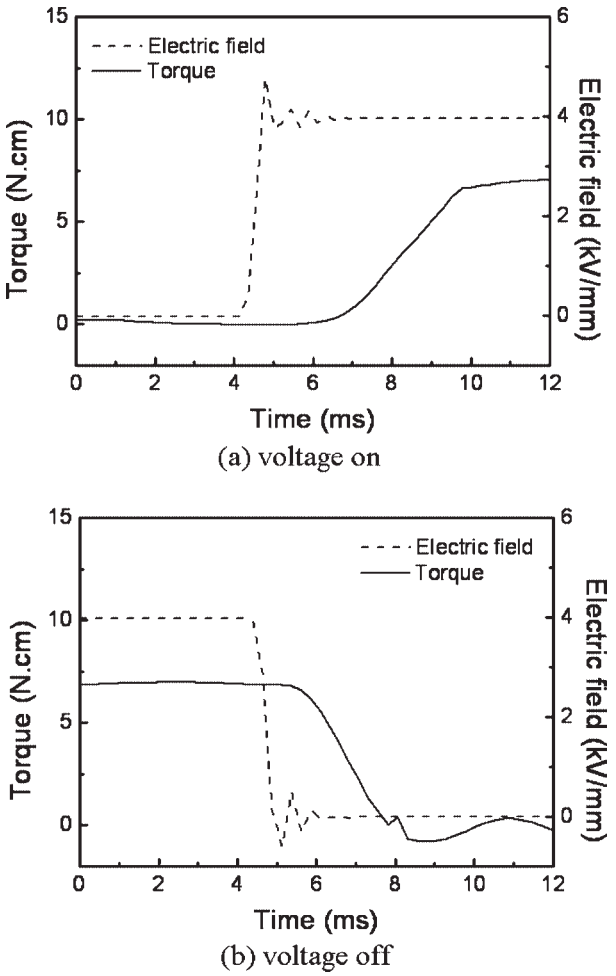

Figure 12 Response time of ERF-2 (25°C).

Figure 10 shows the influence of the electrode materials with ERF-2. Contrary to the results of ERF-1, it can be observed from the results of ERF-2 that similar yield stresses and current densities were obtained at an operating temperature of 25°C, regardless of the electrode material. As the temperature increased to 70°C, the electric fields for the three electrode materials were limited by 3 kV/mm, with a similar increase in the current density. Consequently, the yield stresses of ERF-1 were dependent on the electrode materials, whereas the yield stresses of ERF-2 were constant, regardless of the electrode materials and operating temperature. It can also be observed that the electric fields were restricted by the amount of current density, although the yield stresses at an operating temperature of 70°C were not much higher than those at 25°C.

Figures 11 and 12 present the rising (voltage on) and falling (voltage off) time response characteristics at 25°C, which were measured directly from the test devices shown in Figure 1. An electric field of 4 kV/mm was applied, and the measured shear stress was achieved from the torque transducer with an A/D converter. The shear rate was kept at a constant value of 10 s^{-1}. The response time was obtained by an inspection of the required time when the shear stress reached 63.2% of its final steady-state values. The response time of ERF-1 was evaluated to be 5.9 ms in the rising case and 4.8 ms in the falling case, whereas the rising and falling response times

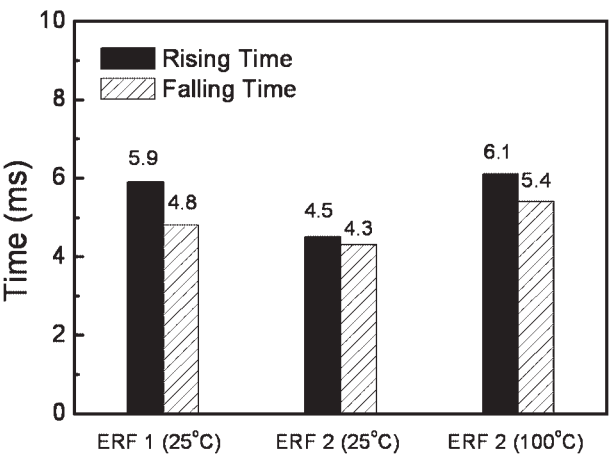

Figure 13 Comparison of the response time (4 kV/mm).

of ERF-2 were 4.5 and 4.3 ms, respectively, as shown in Figures 11 and 12. There was almost no difference in the response time between ERF-1 and ERF-2. It is clearly shown in Figure 13 that the response time of ERF-2 was not affected by temperature variation for either the rising or falling case. ERF-1 and ERF-2 have fast response times that can be applied to a practical device.

CONCLUSIONS

The Bingham characteristics and response characteristics of polymer-based ER fluids with different electrode gaps (0.75, 1.00, and 1.25 mm) and electrode materials (stainless steel, carbon steel, and brass) were experimentally investigated. For ER fluids, a water-based Arabic gum ER fluid (ERF-1) and a dry-based polyurethane ER fluid (ERF-2) were employed. After a shear-mode-type electroviscometer was devised, comparisons of the field-dependent yield stress, current density, and response time were undertaken. It was observed that the yield stresses of ERF-1 and ERF-2 increased with similar (or sometimes even decreasing) current densities as the electrode gap decreased. This means that the smaller electrode gap is more efficient than the larger one because a higher yield stress can be obtained with the same power consumption. The efficiency of the yield stress versus power consumption decreased as the operating temperature increased because applied electric fields are subject to high current densities at a high operating temperature, regardless of the electrode gaps and materials. In addition, the yield stresses of ERF-1 are dependent on the electrode materials, whereas the yield stresses of ERF-2 remain constant, regardless of the electrode materials and operating temperature. It has also been demonstrated that the response time of ERF-1 and ERF-2 is not affected by temperature variations for either the rising or falling cases. The experimental results presented in this work will be very useful for determining the appropriate electrode gap and electrode material for the design of ER devices or mechanisms.

References

1. Kim, D. H.; Kim, Y. D. J Ind Eng Chem 2007, 13, 879.
2. Cheng, Q.; He, Y.; Pavlinek, V.; Lengalova, A.; Li, C.; Saha, P. J Mater Sci 2006, 41, 5047.
3. Winslow, W. H. J Appl Phys 1949, 20, 1137.
4. Jordan, T. C.; Shaw, M. T. IEEE Trans Electrical Insul 1989, 24, 849.
5. Fang, F. F.; Kim, J. H.; Choi, H. J.; Seo, Y. J Appl Polym Sci 2007, 105, 1853.
6. Yilmaz, H.; Unal, H. I.; Sari, B. J Appl Polym Sci 2007, 103, 1058.
7. Kesy, Z.; Kesy, A.; Plocharski, J.; Jackson, M.; Parkin, R. Mechatronics 2006, 16, 33.
8. Choi, S. B.; Han, S. S.; Sung, K. G.; Lee, Y. S.; Han, M. S. Smart Mater Struct 2006, 15, 850.
9. Kamath, G. H.; Hurt, M. K.; Wereley, N. M. Smart Mater Struct 1996, 5, 576.
10. Choi, S. B.; Sung, K. G.; Lee, J. W. J Dyn Syst Trans ASME 2002, 124, 435.
11. See, H.; Mackenzie, S.; Chua, B. J. Korea–Aust Rheol J 2006, 18, 121.
12. Lynch, R.; Meng, Y.; Filisko, E. J Colloid Interface Sci 2006, 297, 322.
13. Jung, W. J.; Jeong, W. B.; Hong, S. R.; Choi, S. B. J Sound Vib 2004, 273, 185.
14. Zhang, Y.; Lu, K.; Rao, G.; Tian, Y.; Zhang, S.; Liang, J. Appl Phys Lett 2002, 80, 888.
15. Chotpattananont, D.; Sirivat, A.; Jamieson, A. M. Polymer 2006, 47, 3568.
16. Choi, H. J.; Kim, J. W.; Joo, J.; Kim, B. H. Synth Met 2001, 121, 1325.
17. Gao, Z. W.; Zhao, X. P. J Appl Polym Sci 2004, 93, 1681.
18. Cho, M. S.; Choi, H. J.; Chin, I. J.; Ahn, W. S. Micropor Mesopor Mater 1999, 32, 233.
19. Sakurai, R.; See, H.; Saito, T. J Rheol 1996, 40, 395.
20. Sung, J. H.; Park, D. P.; Park, B. J.; Choi, H. J.; Jhon, M. S. Biomacromolecules 2005, 6, 2182.
21. Ikazaki, F.; Kawai, A.; Uchida, K.; Kawakami, T.; Edamura, K.; Sakurai, K.; Anzai, H.; Asako, Y. J Phys D 1998, 31, 336.
22. Jang, W. H.; Kim, J. W.; Choi, H. J.; Jhon, M. S. Colloid Polym Sci 2001, 279, 823.
23. Kim, J. W.; Kim, S. G.; Choi, H. J.; Jhon, M. S. Macromol Rapid Commun 1999, 20, 450.
24. Kim, J. W.; Liu, F.; Choi, H. J.; Hong, S. H.; Joo, J. Polymer 2003, 44, 289.
25. Fang, F. F.; Choi, H. J.; Joo, J. J Nanosci Nanotechnol 2008, 8, 1559.
26. Cho, M. S.; Cho, Y. H.; Choi, H. J.; Jhon, M. S. Langmuir 2003, 19, 5875.
27. Kim, S. G.; Lim, J. Y.; Sung, J. H.; Choi, H. J.; Seo, Y. Polymer 2007, 48, 6622.
28. Choi, H. J.; Jhon, M. S. Soft Matter 2009, 5, 1562.
29. Choi, S. B.; Sohn, J. W.; Lee, Y. S. Key Eng Mater 2006, 324, 173.
30. Choi, S. B.; Sung, K. G. Key Eng Mater 2006, 324, 177.
31. Karnopp, D. C.; Crosby, M. J.; Harwood, R. A. ASME J Eng Ind 1974, 96, 619.
32. Choi, S. B.; Sung, K. G. Int J Vehicle Des 2008, 46, 94.
33. Choi, S. B.; Choi, Y. T.; Chang, E. G.; Han, S. J.; Kim, C. S. Mechatronics 1998, 8, 143.
34. Bloodworth, R.; Wendt, E. Int J Modern Phys B 1996, 10, 2951.
35. Jimenez, A. J.; Kostic, M. Rev Sci Instrum 1994, 65, 229.
36. Cho, M. S.; Choi, H. J.; Jhon, M. S. Polymer 2005, 46, 11484.